

# Unsupervised clustering of Southern Ocean Argo float profiles

Daniel C. Jones<sup>1</sup>, Harry J. Holt<sup>1,2</sup>, Andrew J.S. Meijers<sup>1</sup>, Emily Shuckburgh<sup>1</sup>

<sup>1</sup>British Antarctic Survey, Cambridge, UK

<sup>2</sup>Department of Physics, University of Cambridge, Cambridge, UK

## Key Points:

- We apply Gaussian mixture modeling (GMM) to Southern Ocean temperature and salinity data
- GMM identifies spatially coherent profile types without using latitude or longitude information

---

Corresponding author: D. C. Jones, [dannes@bas.ac.uk](mailto:dannes@bas.ac.uk)

## 11 Abstract

12 The Southern Ocean features a complex density structure characterised by sharp fronts,  
 13 deep seasonal mixed layers, water mass formation regions, and salt-stratified waters, car-  
 14 rying the imprints of the Antarctic Circumpolar Current, gyre circulation, overturning,  
 15 and mixing. Methods of characterising Southern Ocean density structures traditionally  
 16 rely on somewhat ad-hoc definitions based on physical, chemical, and dynamic proper-  
 17 ties. As an alternative approach, here we apply an unsupervised classification technique  
 18 (i.e. Gaussian mixture modelling) to Southern Ocean Argo float profiles. Gaussian mix-  
 19 ture modelling, without using any latitude or longitude information, automatically iden-  
 20 tifies several circumpolar classes, as well as classes that bear the imprint of mode/intermediate  
 21 water formation and export, large-scale gyre circulation, and the Agulhas Current.

## 22 1 Introduction

23 The Southern Ocean is a critical component of Earth’s climate system, having thus  
 24 far absorbed greater than 75% of the energy added via anthropogenic emissions and 50%  
 25 of the excess carbon [Fletcher *et al.*, 2006; Frölicher *et al.*, 2015]. Its ability to absorb  
 26 heat and carbon comes in part from its unique density structure and circulation, which  
 27 features upwelling of cold, nutrient rich waters and dense water formation regions [Lump-  
 28 kin and Speer, 2007]. Characterising and understanding the mean state and variability  
 29 of Southern Ocean density structure remains an important and climatically-relevant goal  
 30 of modern oceanography.

31 Through decades of effort, the oceanographic community has converged on a de-  
 32 scription of ocean structure that uses temperature, salinity, dynamical, and biogeochem-  
 33 ical patterns to define different water masses (e.g. using potential vorticity minima to  
 34 locate mode water pools) [Talley, 2013, and references therein]. This scheme exploits the  
 35 understanding that water mass properties are “set” in their formation regions and mod-  
 36 ified by advection, mixing, and biogeochemical processes. This modern classification scheme  
 37 is extremely useful and will continue to be useful well into the future, but it is not nec-  
 38 essarily ideal for every application. Many of the temperature, salinity, and density val-  
 39 ues used to delimit one water mass from another are somewhat ad-hoc and very specific  
 40 (e.g. boundaries between different types of mode water), such that they are useful for  
 41 observational data analysis but difficult to apply to numerical models of the ocean, which  
 42 do not necessarily feature exactly the same structure as the observed ocean [Sallée *et al.*,

2013]. It is therefore prudent to develop and test alternative methods for the classification of different oceanic temperature, salinity, and density structures, as a complement to existing expertise-driven methods.

*Maze et al.* [2017] have shown that Argo profile data from the North Atlantic Ocean can be usefully grouped into classes using Gaussian mixture modelling (GMM), an unsupervised classification technique. GMM describes the spatial structure of Argo profiles by as a collection of Gaussian models whose means and standard deviations generally vary with depth. In this work, we apply GMM to Southern Ocean Argo data in the upper 1000 m of the water column. We find that GMM identifies several circumpolar classes, gyres, salt stratified regions, the Agulhas current, and pathways broadly associated with the formation and export of mode and intermediate waters. In addition, GMM identifies fronts as boundaries between classes and may thus present an alternative method for front location and analysis. In section 2 we describe the Argo dataset and the basics of GMM. In section 3, we present the results of applying GMM to Southern Ocean Argo data, and in section 4 we summarize our conclusions.

## 2 Methods

We applied an unsupervised classification method (i.e. Gaussian mixture modelling, hereafter GMM) to Southern Ocean Argo float data. In this section, we briefly describe the Argo dataset that we used and the basics of GMM. We use the scikit-learn machine learning library for Python (<http://scikit-learn.org/>), and the source code used for much of the analysis in this paper is available via Github (<https://github.com/DanJonesOcean/OceanClustering>). We refer the reader to *Maze et al.* [2017] for further detail on applying GMM to Argo float data.

### 2.1 Argo float dataset

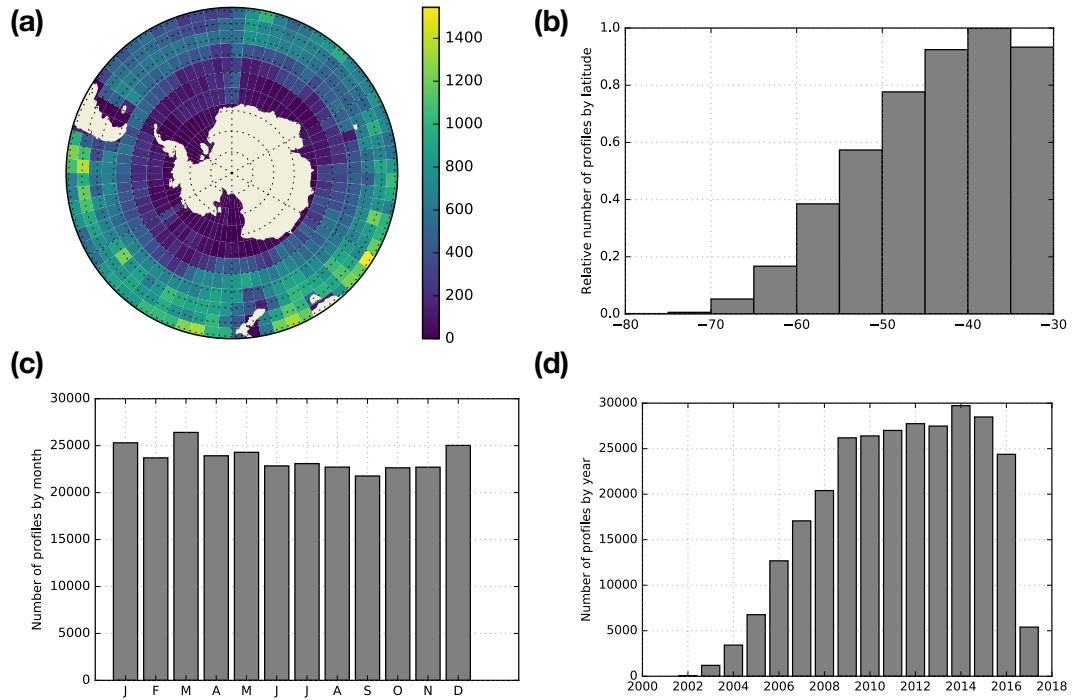
Argo floats are autonomous ocean instruments that measure, at minimum, the temperature and salinity of the ocean by periodically taking vertical profiles. Every 10 days, starting at a “neutral” position of 1000 m, an Argo float dives down to 2000 m before rising to the surface, taking a vertical profile of the water column along the way. The measurements are transmitted via satellite and are ultimately made freely available via the Argo Global Data Assembly Centers (GDACs) after some quality control checks. At

73 the time of this writing, over 3800 Argo floats are active in the global ocean, producing  
74 over 100,000 temperature and salinity profiles per year with an average spacing of  $3^\circ$  (<http://www.argo.ucsd.edu/>).  
75

76 For this study, we selected all available Argo profiles south of  $30^\circ\text{S}$  that have been  
77 flagged by the GDACs as “observation good” (i.e. quality control flag = 1) covering the  
78 time period from 2001 to early 2016. More specifically, we used a vertically interpolated  
79 product with 400 pressure/depth levels ranging from 0 to 2000 dbar. After discarding  
80 profiles with  $\geq 6\%$  NaN values (2% of the initial number of profiles) and discarding  
81 depth levels with  $\geq 3\%$  NaN values, we were left with 284,427 profiles, each with 192  
82 pressure levels between 15 dbar and 980 dbar. We replaced all remaining NaN values ( $\ll$   
83 1% of the total temperature measurements) with linearly interpolated estimates using  
84 nearest neighbor values. We refer to the resulting dataset as the “cleaned” dataset.

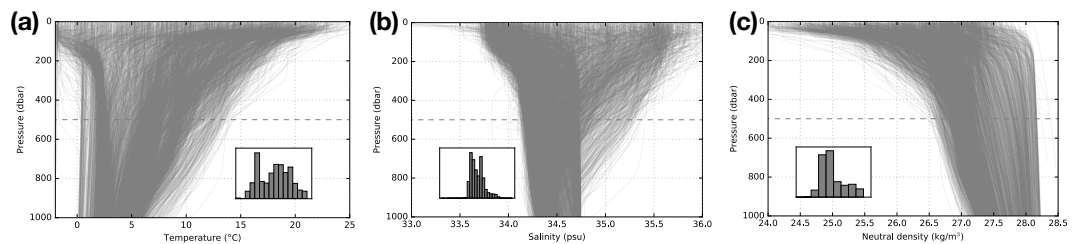
85 Because of the autonomous and free-drifting nature of the floats, the profiles are  
86 not distributed evenly in latitude/longitude (Figure 1). The profiles are more heavily con-  
87 centrated in the Pacific sector (roughly 890 profiles per degree longitude, totalling 47%  
88 of profiles) and Indian sector (800 profiles per degree longitude, totalling 34% of profiles),  
89 with relatively fewer profiles in the Atlantic sector (610 profiles per degree longitude, 19%  
90 of total). When counted in equal-area bins and plotted by latitude, we see that the num-  
91 ber of profiles decreases towards Antarctica (Figure 1(b)), which is partly due to chal-  
92 lenging operational conditions associated with seasonal sea ice, which can extend to just  
93 north of  $60^\circ\text{S}$  at maximum areal extent. The profiles are slightly over-represented in the  
94 Austral summer and autumn (DJF-MAM, 52% of profiles) and under-represented in the  
95 Austral winter and spring (JJA-SON, 48% of profiles), and the number of profiles increases  
96 until 2013 (Figure 1(c,d)). The relatively low number of profiles used in 2016 reflects the  
97 time when the particular dataset chosen for this study was generated and does not re-  
98 flect a lack of profiles in the total Argo dataset.

103 The profiles selected for this study display a large variety of vertical temperature  
104 structures (Figure 2). The range of temperatures is much larger in the surface and con-  
105 siderably narrower at depth, in part reflecting the seasonal cycle in upper ocean tem-  
106 peratures. A large number of profiles feature colder temperatures near the surface and  
107 warmer temperatures in the interior, which on its own is physically unstable to convec-  
108 tion. However, water masses around Antarctica tend to be fresher at the surface and saltier



99 **Figure 1.** Distribution of Argo profiles from the cleaned dataset. (a) Number of profiles in  
 100  $5^\circ \times 5^\circ$  bins. (b) Relative number of profiles by latitude, scaled by an area-weighting factor  
 101  $\cos(\phi)$ , where  $\phi$  is the latitude. The temporal distribution of profiles shown by (c) month and (d)  
 102 year.

109 in the interior due to glacial melt, freshwater flux, and the balance of evaporation/precipitation.  
 110 This arrangement of temperature and salinity can be stable to vertical mixing (called  
 111 “salt stratification”). In addition, the thermocline, i.e. the region of the ocean that fea-  
 112 tures a rapid change in temperature with depth, is visible in some temperature profiles.



113 **Figure 2.** Histogram of Argo (a) temperature profiles and (b) salinity profiles in the cleaned  
 114 dataset. Neutral density profiles (c) are derived from temperature and salinity. Only 10% of the  
 115 profiles are shown for visibility, and pressure levels below 1000 dbar were discarded.

## 116 2.2 Gaussian mixture modeling

117 Gaussian mixture modeling (GMM) is a probabilistic approach to describing and  
 118 classifying data. It attempts to fit (or “model”) the data as a linear combination of multi-  
 119 dimensional Gaussian distributions with unknown means and unknown standard devi-  
 120 ations. Let  $\mathbf{X}$  be the array of  $N$  vertical profiles, each with  $D$  pressure/depth levels, and  
 121 let  $p(\mathbf{X})$  be the probability distribution function (PDF) representing the entire dataset.  
 122 GMM represents the PDF as a weighted sum of  $k$  Gaussian classes, indexed by  $c$ , i.e.:

$$p(\mathbf{X}) = \sum_{c=1}^k \lambda_c \mathcal{N}(\mathbf{X}; \mu_c, \Sigma_c). \quad (1)$$

123 Here,  $k$  is the total number of Gaussian distributions/classes used in the model and  $\mathcal{N}(\mathbf{x}; \mu_c, \Sigma_c)$   
 124 is the multi-dimensional Gaussian (i.e. normal) PDF with a vector of means  $\mu_c$  and co-  
 125 variance matrix  $\Sigma_c$ , i.e.:

$$\mathcal{N}(\mathbf{x}; \mu_c, \Sigma_c) = \frac{\exp\left[-\frac{1}{2}(\mathbf{x} - \mu_c)^T \Sigma_c^{-1}(\mathbf{x} - \mu_c)\right]}{\sqrt{(2\pi)^D |\Sigma_c|}}. \quad (2)$$

126 The probability associated with class/component  $c_a$  is  $p(c = c_a) = \lambda_{c_a}$ . The proba-  
 127 bility of profile  $\mathbf{x}$  being in class/component  $c_a$  is  $p(\mathbf{x}|c = c_a) = \mathcal{N}(\mathbf{x}; \mu_{c_a}, \Sigma_{c_a})$ , where  
 128 the vector  $\mathbf{x}$  is a single profile taken from the complete array  $\mathbf{X}$ . Both  $\mathbf{x}$  and  $\mu_c$  are vec-  
 129 tors of length  $D$ .

130 Starting with random initial guesses for the classes, GMM proceeds by iteratively  
 131 adjusting the means  $\mu_c$  and standard deviations  $\Sigma_c$  (i.e. the “parameters”) of the classes  
 132 in order to maximize a logarithmic measure of likelihood, i.e.:

$$\log[p(\mathbf{X})] = \sum_i \log \left[ \sum_{c=1}^k \lambda_c \mathcal{N}(\mathbf{X}; \mu_c, \Sigma_c) \right], \quad (3)$$

133 It does so following an expectation-maximization approach, described in *Maze et al.* [2017].  
 134 This algorithm monotonically converges on a local maximum. GMM is a generalization  
 135 of  $k$ -means clustering, which only attempts to minimize in-group variance by shifting the  
 136 means. By contrast, GMM attempts to identify means and standard deviations, allow-  
 137 ing for some variation about the centres of the Gaussian distributions.

138 In our instance of GMM, each depth level is treated as a “dimension” with Gaus-  
 139 sian parameters associated with each depth level. However, we may not need all of these  
 140 depth levels to accurately describe the dataset, as ocean temperature changes much more  
 141 rapidly in the mixed layer and thermocline than in the relatively quiescent interior. In  
 142 order to reduce the computational complexity of the problem, we transform the profile

143 data from pressure/depth space to an alternative space using principal component anal-  
 144 ysis (PCA). Specifically, we calculate principal components that capture a desired frac-  
 145 tion of the vertical variability of the dataset. Each eigenvector may be thought of as a  
 146 “profile type” that describes a certain amount of variance in the data with depth (note  
 147 that this is not necessarily the same thing as a “typical profile”). We calculate  $d$  prin-  
 148 cipal components and employ the transformation:

$$\mathbf{X}(z) = \sum_{j=1}^d \mathbf{P}(z, j) \mathbf{Y}(j), \quad (4)$$

149 where  $z$  is the depth level,  $d$  is the total number of principal components (index  $j$ ), and  
 150  $\mathbf{P}(z, j)$  is the transformation matrix between pressure/depth space and principal com-  
 151 ponent space. We find that  $d = 6$  captures 99.9% of the variance in the vertical struc-  
 152 ture, which greatly reduces the number of dimensions needed to describe the Argo pro-  
 153 file data used here, i.e. from 194 pressure/depth levels to 6 principal components.

154 GMM does have one free parameter, i.e. the maximum number of classes  $k$ . In or-  
 155 der to determine the most appropriate value for  $k$ , we applied two statistical tests, namely  
 156 (i) a Bayesian Information Criterion (BIC) and (ii) a Variational Bayesian GMM (VB-  
 157 GMM) test. The first test (BIC) uses an empirically formulated cost function that re-  
 158 wards likelihood and penalizes the number of classes  $k$ :

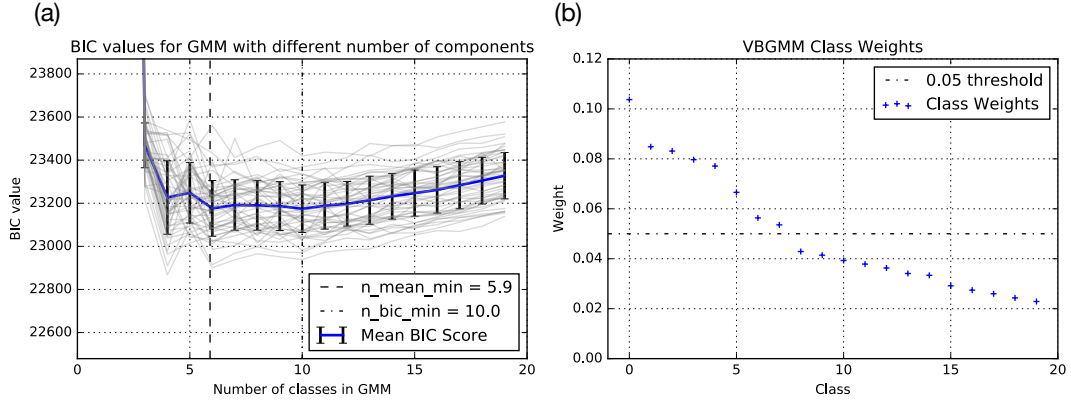
$$BIC(k) = -2\mathcal{L}(k) + N_f(k) \log(n), \quad (5)$$

159 where  $\mathcal{L}$  is a measure of likelihood,  $n$  is the number of profiles used in the BIC test, and  
 160  $N_f$  is the number of independent parameters to be estimated:

$$N_f(k) = k - 1 + kD + \frac{kD(D-1)}{2}. \quad (6)$$

161 The decorrelation scale in the Southern Ocean is approximately 300 km [*Ninove et al.*,  
 162 2016]. Using this 300 km scale as guidance, we randomly select a profile from each  $4^\circ \times$   
 163  $4^\circ$  grid cell, returning 884 random profiles for each BIC test. We calculate BIC scores  
 164 for each set of 884 random profiles (in principal component space) using a range of classes  
 165  $k$  from 1 to 19 (Figure 3(a)). Although BIC does not return a clear, single minimizer  $k_{min}$ ,  
 166 it suggests that the optimum  $k_{min}$  value lies between 6 and 10.

174 As a complement to BIC, we also used VB-GMM to determine the optimum num-  
 175 ber of classes  $k$ , available as a function within scikit-learn. This clustering method as-  
 176 signs a weight to each class. Based on this test, we choose  $k = 8$ , as higher values of



167 **Figure 3.** (a) Bayesian Information Criteria (BIC) scores versus the specified number of  
 168 classes  $k$ . Shown are the individual trials for different subsets of the temperature profile datasets  
 169 (grey lines), the mean (blue line), and standard deviations computed from the profiles. The  
 170 dashed line represents the average of the minimums from each profile and the dash-dot line repre-  
 171 sents the minimum of the average of the profiles. (b) Class weights from VB-GMM with up to 20  
 172 components, indexed from 0 to 19. The dash-dot line is a line of equal probability for 20 classes  
 173 0.05.

177  $k$  fall below the level of equal probability (0.05 for 20 classes) (Figure 3(b)). In addition,  
 178 our choice of  $k = 8$  is partly informed by the value that returns a physically useful de-  
 179 scription of ocean structure.

180 Clustering algorithms organise data into groups or sets according to a defined rule,  
 181 ideally identifying structures in the dataset. Oceanography has a rich history of expertise-  
 182 driven clustering using physical and biogeochemical criteria (e.g. PV minima, oxygen  
 183 minima), fingerprints of physical and biogeochemical processes, and identifiable patterns.  
 184 These descriptions can be arranged into hierarchies, from coarse/simple (e.g. two-layer  
 185 quasi-geostrophic models) to rich and complex (e.g. the descriptions found in *Talley* [2013]),  
 186 where the level of detail required in the description depends on the application at hand.  
 187 For example, a simple  $\beta$ -plane model is sufficient to explain the existence of gyres and  
 188 western boundary currents; it constitutes a first-order description of gyres. Algorithmic  
 189 clustering offers a robust way to traverse this hierarchy. As we have seen, BIC and VB-  
 190 GMM suggest that the optimum number of classes is between 6 and 10. Although these  
 191 statistical tests can be used as a rough guide for choosing the number of classes, there  
 192 is not necessarily a single “correct/ideal” value for  $k$ , which can be thought of as a weakly



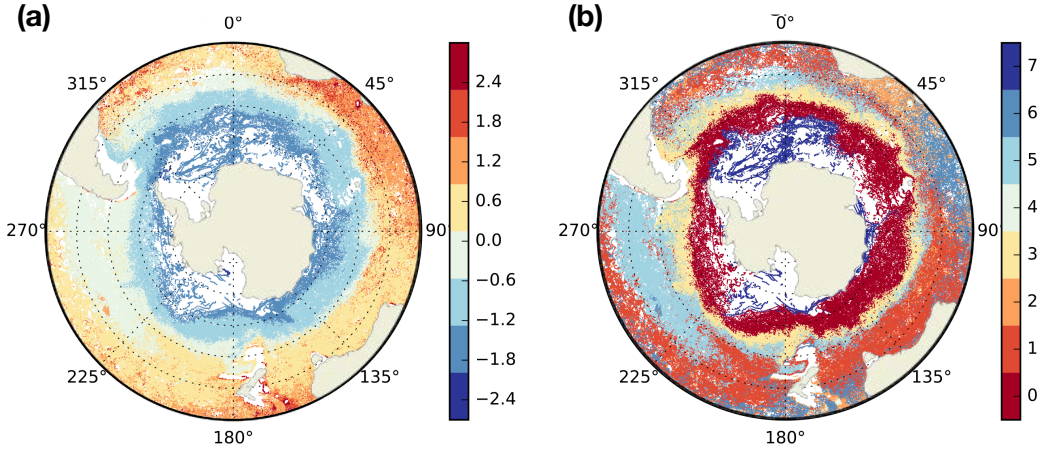
193 constrained parameter indicating the level of complexity in the statistical description of  
 194 the dataset. We explore the impact of  $k$  on our results in the appendix.

195 Below we refer to “training” datasets and “test” datasets. Both are subsets of the  
 196 cleaned dataset. BIC and GMM generally use different training datasets. For the GMM  
 197 training set, we randomly selected a single profile from each  $1^\circ \times 1^\circ$  bin. Each train-  
 198 ing dataset contains 12,286 profiles (roughly 4% of the cleaned dataset), distributed evenly  
 199 in latitude/longitude space. The training dataset is used to estimate the parameters (i.e.  
 200 the means and standard deviations) of the GMM classes, and the fitted Gaussian model  
 201 with optimized parameters is then applied to the test dataset. The end result is a prob-  
 202 abilistic description of the cleaned Argo dataset in terms of a linear combination of Gaus-  
 203 sian distributions that vary with depth.

### 204 **3 Results**

205 We describe the cleaned Argo temperature profiles as a linear combination of multi-  
 206 dimensional Gaussian functions in order to identify patterns in the temperature struc-  
 207 ture of the Southern Ocean. As an initial test, we start with a simple one-dimensional  
 208 case by clustering vertical mean temperatures. The GMM algorithm identifies spatially-  
 209 coherent patterns, despite not having access to the longitudes or latitudes of the profiles  
 210 (Figure 4). On the basin-scale, GMM identifies patterns that roughly correspond to some  
 211 physically familiar temperature structures. For instance, there are several circumpolar  
 212 classes (labeled 0, 3, and 7), consistent with the tendency of the Antarctic Circumpo-  
 213 lar Current (ACC) to homogenize properties along its streamlines. The circumpolar class  
 214 closest to Antarctica (class 7) also extends throughout the Weddell Gyre. Having shown  
 215 that GMM can identify spatially coherent structures without using latitude/longitude  
 216 data, we turn our attention to vertical variations in temperature.

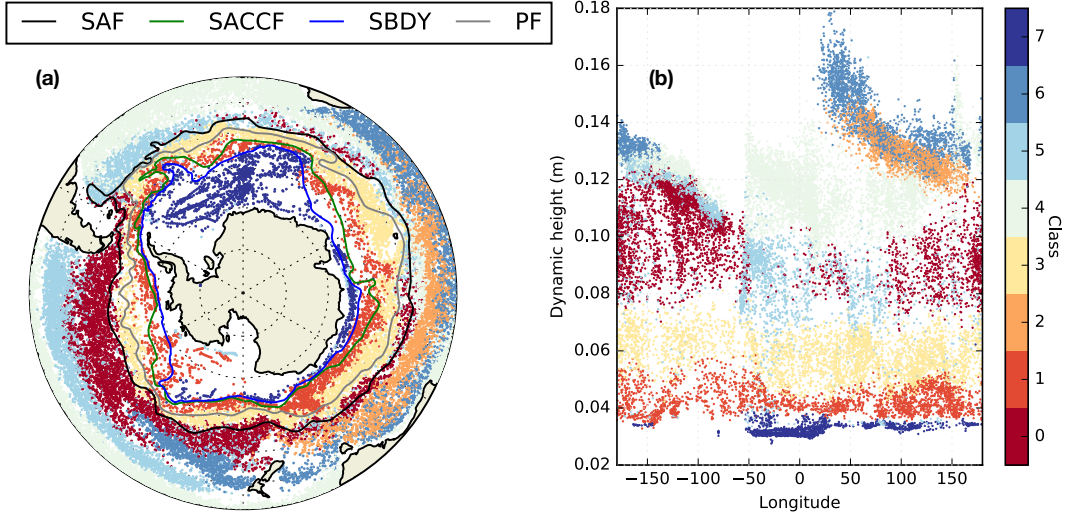
219 We classify Argo profiles from our “cleaned” dataset into  $k = 8$  different clusters,  
 220 and as with the vertical mean temperature case, we find spatially coherent structures  
 221 (Figure 5). The class nearest Antarctica (class 7) extends throughout the Weddell Gyre  
 222 and around coastal Antarctica. The mean profiles in this region tend to be salt strat-  
 223 ified. The near-Antarctic class coincides with regions of deep water formation and up-  
 224 welling of dense water, and its northern boundary coincides with the classical “south-  
 225 ern boundary” front (SBDY) of the Antarctic Circumpolar Current. This class occupies



217 **Figure 4.** (a) Vertically averaged temperature anomaly (C) relative to the domain mean. (b)  
 218 GMM classes for vertical mean temperature, calculated with  $k = 8$ .

226 a narrow range in dynamic height space and is fairly distinct from the other classes (i.e.  
 227 profiles of this class type are very rarely found north of the classical southern boundary),  
 228 indicating that GMM has identified a cluster that is physically distinct and identifiable.

229 North of the SBDY, GMM identifies two circumpolar classes (classes 1 and 3). The  
 230 southernmost circumpolar class (class 1) is located south of the Polar Front (PF) and  
 231 is consistent with the homogenizing tendency of ACC circulation. The second circumpolar  
 232 class (class 3) is mostly located south of the classical SAF. As with the near-Antarctic  
 233 class, classes 1 and 7 occupy distinct regions when plotted in dynamic height space at  
 234 all longitudes, indicating that they are indeed physically separate from the others. Class  
 235 0 is located just north of the SAF in the Pacific and Indian sectors. Together with the  
 236 Pacific component of class 5, these two clusters roughly coincide with broad patterns as-  
 237 sociated with the formation and export of Subantarctic Mode Water and Antarctic In-  
 238 termediate Water, both of which may impact the temperature structure of the local wa-  
 239 ter column [Judicone et al., 2007; Jones et al., 2016]. Similarly, class 2 is spatially co-  
 240 incident with the westward export pathway of mode water formed in the deep mixed lay-  
 241 ers south of Australia [Jones et al., 2016, Fig. 4b]. GMM identifies a class that overlaps  
 242 with the Agulhas current and retroflexion (class 6), although in dynamic height space  
 243 this class overlaps with others. Profiles in class 6 are also found east of New Zealand.  
 244 Class 4 is associated with subtropical water and represents the lowest-latitude profiles  
 245 in the Atlantic and Pacific basins.

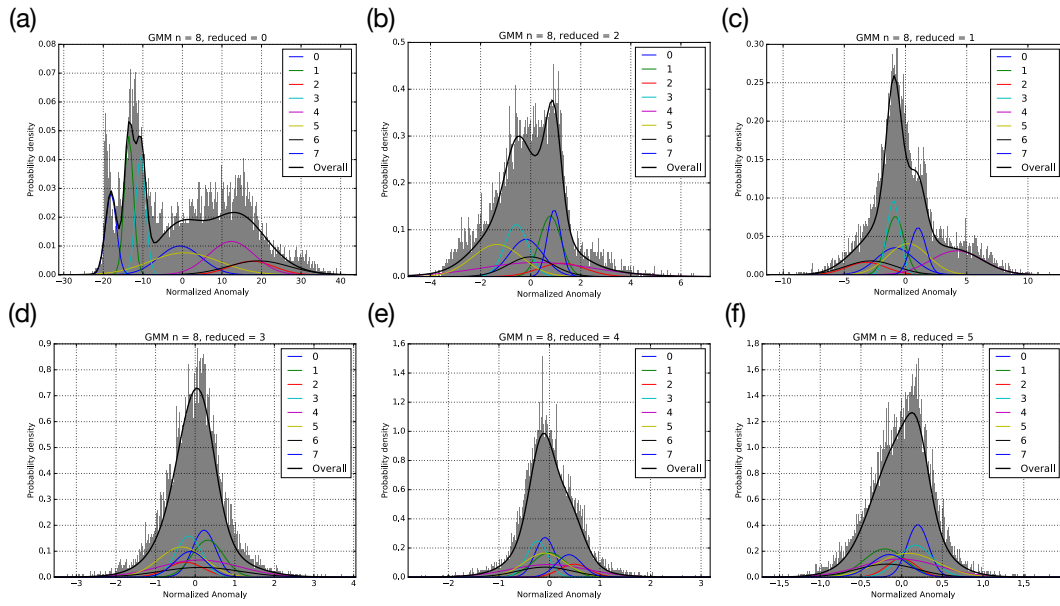


246 **Figure 5.** (a) GMM-derived class distribution for  $k = 8$ , shown with four fronts of the Antarc-  
 247 tic Circumpolar Current, i.e. the Subantarctic Front (SAF), Southern ACC Front (SACCF),  
 248 Southern Boundary (SBDY), and the Polar Front (PF). (b) Class distribution shown in dynamic  
 249 height space. Note that only points with posterior probability  $\geq 0.9$  are shown.

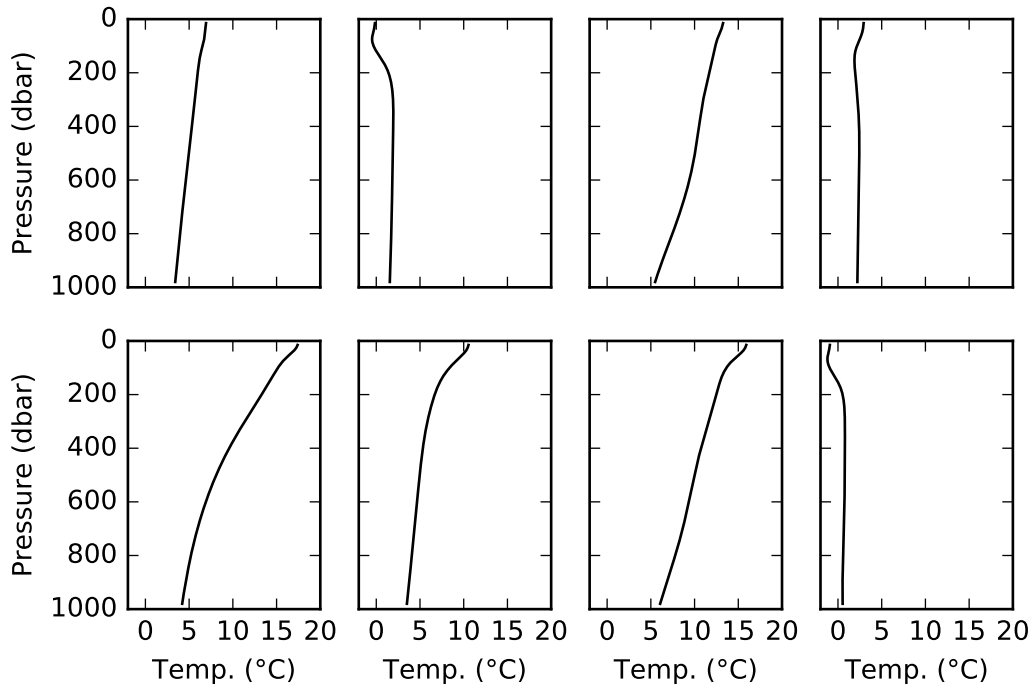
250 In order to classify the Argo profiles based on their vertical structures, we applied  
 251 GMM to the centered, standardized training dataset in principal component (PC) space.  
 252 Although direct physical interpretation of the fits in PC space is difficult, we see that  
 253 the  $k = 8$  component Gaussian distribution is able to capture the broad features of the  
 254 values associated with each principal component (Figure 6). The Gaussians are more dis-  
 255 tinct and spread out for the first three principal components, whereas the higher indexed  
 256 PCs feature more overlap between Gaussian classes.

259 The mean temperature profiles associated with each class show several different types  
 260 of vertical temperature profiles (Figure 7). We see three inverted profiles that are cooler  
 261 near the surface and warmer with depth. These correspond to salt stratified profiles, i.e.  
 262 where the vertical stability of the profile relies on the salt distribution, which is neces-  
 263 sarily a fresh surface layer overlying a denser, saltier interior. Many of these profiles can  
 264 be found in the Weddell Sea and near the wider Antarctic shelf. Other classes feature  
 265 a decrease in temperature from the surface into the interior, with different means and  
 266 vertical structures.

268 One advantage of GMM over k-means clustering is that GMM returns posterior  
 269 probabilities, i.e. measures of the likelihood of each class assignment (Figure 8). On basin



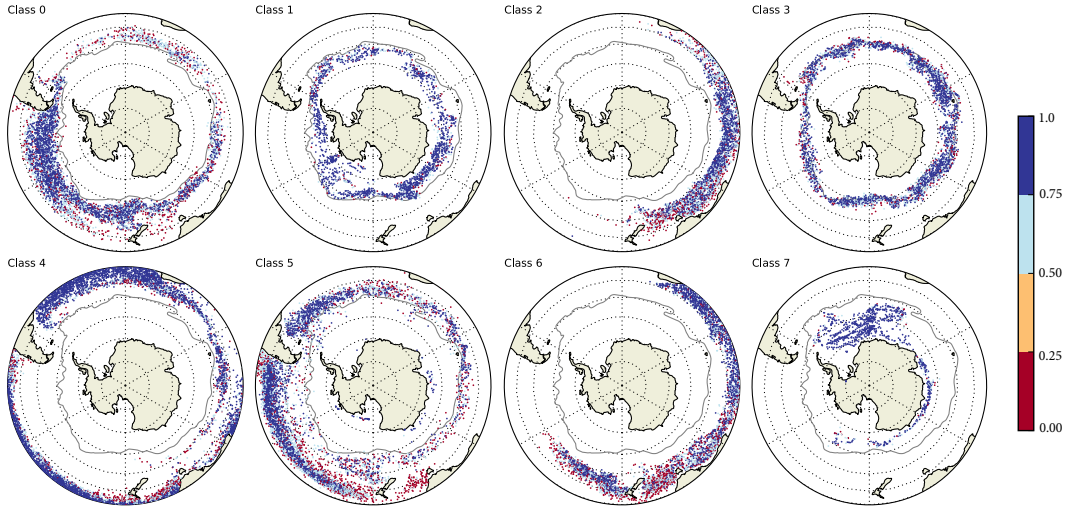
257 **Figure 6.** Probability density functions for each principal component (referred to as “reduced  
 258 depth levels” in the plot). For each principal component, each Gaussian component is shown.



267 **Figure 7.** GMM class mean temperature profiles with depth.

270 scales, the posterior probabilities associated with each of the 8 classes is above 0.8, which  
 271 quantifies the likelihood that the classes have been assigned to the most suitable class.

272 Many of the regions in which the posterior probabilities are low correspond to regions  
 273 of strong mixing, although low sampling may affect the probabilities as well. We also find  
 274 probabilities less than 0.8 at the boundaries between classes, indicating the degree of rel-  
 275 ative smoothness of transitions between different class types.



276 **Figure 8.** Posterior probabilities for the 8 classes, shown together with the Polar Front of the  
 277 ACC.

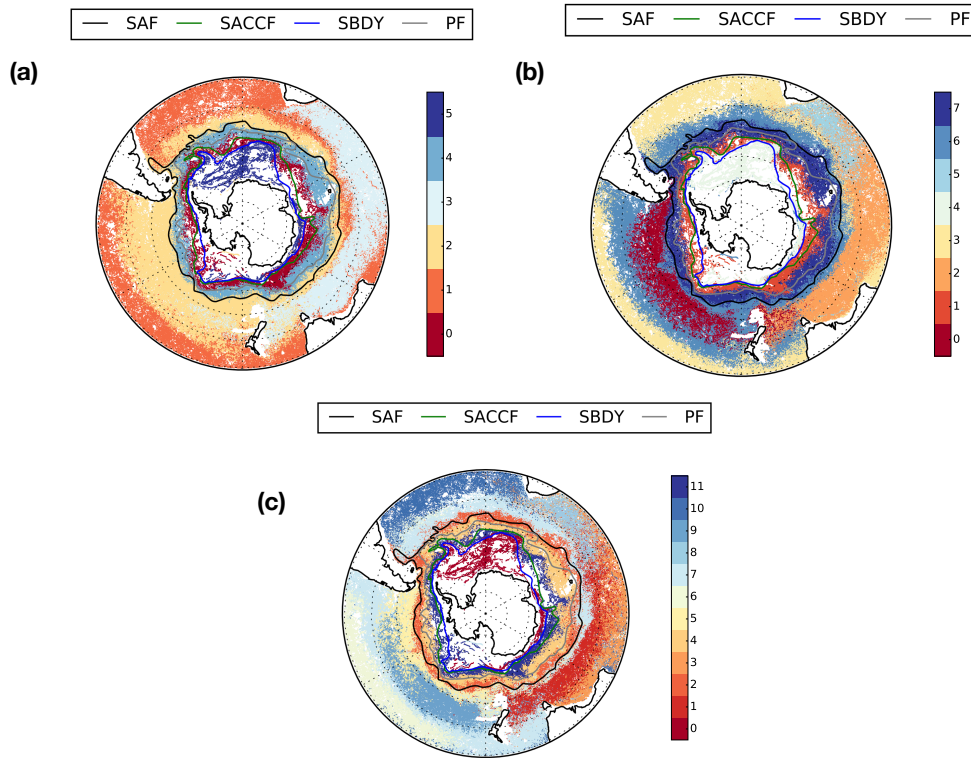
## 278 4 Conclusions

279 We applied Gaussian Mixture Modeling (GMM), an unsupervised classification scheme,  
 280 to Southern Ocean Argo float data above 1000 m. Without using longitude or latitude  
 281 information, GMM identified spatially coherent patterns in the vertical temperature struc-  
 282 ture. The GMM-derived classes broadly coincide with large-scale circulation and strat-  
 283 ification features, including regions of bottom water formation and upwelling (i.e. ad-  
 284 jacent to Antarctica), the Antarctic Circumpolar Current, formation and export path-  
 285 ways of Subantarctic Mode Water and Antarctic Intermediate Water, subtropical gyre  
 286 circulation, and the Agulhas Current and associated retroflexion. The class boundaries  
 287 broadly coincide with several classically-defined fronts of the ACC, and the circumpo-  
 288 lar classes occupy distinct regions in dynamic height space, indicating that GMM has  
 289 identified physically distinct profile types using only vertical temperature data. Poste-  
 290 rior probability distributions indicate regions where the classes are distinct and statis-  
 291 tically separate, whereas regions with low posterior probability indicate boundaries be-

292 tween classes and/or regions of mixing influenced by a number of different temperature  
 293 structures. GMM offers an alternative, complementary method for classification of South-  
 294 ern Ocean density structures.

### 295 **A: Sensitivity to number of classes $k$**

296 In this work, the number of classes  $k$  is constrained between 6 and 10. This weak  
 297 constraint allows for some tuning depending on the desired level of complexity in the de-  
 298 scription of the dataset. Using  $k = 6$  classes is sufficient to capture most of the large-  
 299 scale structures identified in the  $k = 8$  case, except that (1) the cluster found in the  
 300 Agulhas retroflection region and in the area east of New Zealand (class 5 for  $k = 8$ ) is  
 301 grouped together with the Indian-Australian cluster that is spatially coincident with mode  
 302 water formation and export (class 3 for  $k = 6$ ) and (2) the cluster in the Pacific that  
 303 spatially coincides with a region of mode water formation and export (classes 0 and 6  
 304 for  $k = 8$ ) only contains one class instead of two (class 2 for  $k = 6$ ). Moving from  $k =$   
 305 8 to  $k = 12$ , several classes get split into smaller clusters, e.g. the class overlapping the  
 306 Pacific mode waters splits into eastward and westward components, the class south of  
 307 Australia splits into northern/southern components (Figure A.1(c)). The Weddell Sea  
 308 case is identifiable for  $k$  between 6 and 12. The number of circumpolar classes on and  
 309 south of the Polar Front increases from 2 to 3 as we increase  $k$  from 8 to 12. Values of  
 310  $k$  much smaller than 6 or much larger than 12 lose many of the characteristic fingerprints  
 311 of the large-scale circulation processes discussed here (e.g. the along-streamline homog-  
 312 enization enforced by the circulation of the ACC).



313 **Figure A.1.** Comparison of GMM-derived classes, shown for (a) 6 classes, (b) 8 classes,  
 314 (c) 12 classes. Also shown are classically-defined fronts of the Antarctic Circumpolar Current.

315 **Acronyms**

316 **AAIW** Antarctic Intermediate Water

317 **ACC** Antarctic Circumpolar Current

318 **ARGO** Array for Real-time Geostrophic Oceanography

319 **BIC** Bayesian Information Criterion

320 **GDAC** Global Data Assembly Center

321 **GMM** Gaussian mixture modeling

322 **PCA** Principal component analysis

323 **PDF** Probability distribution function

324 **SAMW** Subantarctic Mode Water

325 **VB-GMM** Variational Bayesian Gaussian mixture modelling

## Acknowledgments

This study is supported by grants from the Natural Environment Research Council (NERC), including [1] The North Atlantic Climate System Integrated Study (ACSIS) [grant NE/N018028/1 (authors DJ, ES)] and [3] Ocean Regulation of Climate by Heat and Carbon Sequestration and Transports (ORCHESTRA) [grant NE/N018095/1 (authors EB, AM)]. HH was funded by a NERC DTP Research Experience Placement over the summer of 2017 [grant NE/L002434/1]. Argo float data is freely available for download at <http://www.argo.ucsd.edu/>. The analysis software used in this manuscript was written using Python and the scikit-learn machine learning library (<http://scikit-learn.org/stable/>). The scripts we used are available via github (<https://github.com/DanJonesOcean/OceanClustering>). We are grateful to J.-B. Sallée for front data for the Antarctic Circumpolar Current.

## References

- Fletcher, S. E. M., N. Gruber, A. R. Jacobson, S. C. Doney, S. Dutkiewicz, M. Gerber, M. Follows, F. Joos, K. Lindsay, D. Menemenlis, A. Mouchet, S. A. Müller, and J. L. Sarmiento (2006), Inverse estimates of anthropogenic CO<sub>2</sub> uptake, transport, and storage by the ocean, *Global Biogeochemical Cycles*, *20*(2), doi:10.1029/2005gb002530.
- Frölicher, T. L., J. L. Sarmiento, D. J. Paynter, J. P. Dunne, J. P. Krasting, and M. Winton (2015), Dominance of the Southern Ocean in Anthropogenic Carbon and Heat Uptake in CMIP5 Models, *Journal of Climate*, *28*(2), 862–886, doi:10.1175/jcli-d-14-00117.1.
- Iudicone, D., K. Rodgers, R. Schopp, and G. Madec (2007), An exchange window for the injection of Antarctic Intermediate Water into the South Pacific, *Journal of Physical Oceanography*, *37*, 31–49, doi:<http://dx.doi.org/10.1175/JPO2985.1>.
- Jones, D. C., A. J. S. Meijers, E. Shuckburgh, J.-B. Sallée, P. Haynes, E. K. McAulfield, and M. R. Mazloff (2016), How does Subantarctic Mode Water ventilate the Southern Hemisphere subtropics?, *Journal of Geophysical Research - Oceans*, *121*(9), 6558–6582, doi:10.1002/2016jc011680.
- Lumpkin, R., and K. Speer (2007), Global ocean meridional overturning, *Journal of Physical Oceanography*, *37*, 2550–2562, doi:10.1175/JPO3130.1.
- Maze, G., H. Mercier, R. Fablet, P. Tandeo, M. L. Radcenco, P. Lenca, C. Feucher, and C. Le Goff (2017), Coherent heat patterns revealed by unsupervised classi-



- 358        fication of Argo temperature profiles in the North Atlantic Ocean, *Progress in*  
359        *Oceanography*, *151*, 275–292, doi:10.1016/j.pocean.2016.12.008.
- 360        Ninove, F., P. Y. Le Traon, E. Remy, and S. Guinehut (2016), Spatial scales of tem-  
361        perature and salinity variability estimated from Argo observations, *Ocean Science*,  
362        *12*(1), 1–7, doi:10.5194/os-12-1-2016.
- 363        Sallée, J., E. Shuckburgh, N. Bruneau, A. Meijers, T. Bracegirdle, Z. Wang, and  
364        T. Roy (2013), Assessment of Southern Ocean water mass circulation and char-  
365        acteristics in CMIP5 models: historical bias and forcing response, *Journal of*  
366        *Research: Oceans*, *118*, 1830–1844, doi:10.1002/jgrc.20135.
- 367        Talley, L. (2013), Closure of the Global Overturning Circulation Through the Indian,  
368        Pacific, and Southern Oceans: Schematics and Transports, *Oceanography*, *26*(1),  
369        80–97, doi:10.5670/oceanog.2013.07.